COLLEGE OF ENGINEERING
NUCLEAR ENGINEERING & RADIOLOGICAL SCIENCES
UNIVERSITY OF MICHIGAN

Nuclear Reactor
Analysis & Methods
Group
NuRAM

NE/8887/2021-001-00
NURAM-2021-0004-00

Preliminary Passive Feedback Model Development and Integration

Qicang Shen[1] and Brendan Kochunas[1]

[1] *University of Michigan*

06/30/2021

NEUP Nuclear Energy University Program
U.S. Department of Energy

This page is intentionally blank.

REVISION LOG

Revision	Date	Affected Pages	Revision Description
0	06/30/2021	All	Initial Release

Document pages that are:

Export Controlled:	No
IP/Proprietary/NDA Controlled:	No
Sensitive Controlled:	No
Unlimited:	Yes

This work was supported by funding received from the DOE Office of Nuclear Energy's Nuclear Energy University Program under contract number DE-NE0008887.

COLLEGE OF ENGINEERING
NUCLEAR ENGINEERING & RADIOLOGICAL SCIENCES
UNIVERSITY OF MICHIGAN

Argonne NATIONAL LABORATORY

HolosGen™

EXECUTIVE SUMMARY

In this report, we document the investigations of feedback models for the passive control systems being designed as a part of this NEUP project. This work builds on our previous efforts that performed Thermal Hydraulics (TH) analysis of the Holos microreactor with the Systems Analysis Module (SAM) code, and developed Model Predictive Control (MPC) algorithms for control drum system.

This report covers three topics. The first part analyzes the dynamics of the variable flow controllers proposed for a passive reactivity control system. The analysis provides reference results on how much the power can be changed with flow rate change. Our preliminary results show that the flow rate change cannot insert the reactivity instantaneously due to the thermal time constants of graphite. Therefore, the variable flow rate controller is a delayed control system. The MPC algorithm for variable flow rate controller is then developed and analyzed. This step is performed to determine how the flow controller should operate optimally–by assuming we can control it–so that we have requirements for the performance of the passive system that is being designed. Results indicate that the variable flow rate controller can achieve load following for cases where the power ramp rate is smaller than 5% P_0/min with error smaller than 0.1% P_0. These results also agree with our previous expectations. The major challenge for the passive flow rate controller is that a relatively fast flow rate change is required when the power starts or stops changing.

Next we develop a simplified TH model based on a previously developed model for Very High Temperature Reactor (VHTR) designs. The purpose of developing the feedback model is to reduce the computational cost of the TH calculation in the high-fidelity transient neutronics simulation when developing and verifying the control system. The simplified TH model is developed to be consistent with the SAM model in our previous report. The simplified TH model is then verified for a unit cell with the power distribution used in the SAM model. It is shown that the simplified TH model can produce results that agree with SAM results very well with a maximum difference at any point being less than 10 K (which occurs in the graphite). Therefore, we expect that the high-fidelity neutron transport calculation coupled with the simplified TH model to produce reasonably accurate results.

Finally, we lay out the plan for implementing the MPC algorithm in the PROTEUS code. The plan includes forming the model, developing the nonlinear MPC, and developing the basic solvers to solve these problems.

Future work includes implementing the feedback model into the PROTEUS code, and performing coupled high-fidelity simulation. Studying the nonlinear MPC control to see whether it will improve the performance of the control system is another important topic. Eventually, the MPC will be implemented into the PROTEUS code and be used to verify the performance of the semi-autonomous control system.

CONTENTS

LIST OF FIGURES

LIST OF TABLES

ACRONYMS

HTGR High Temperature Gas Reactor

ANL Argonne National Laboratory

SPR Special Purpose Reactor

SPM Subcritical Power Module

MPC Model Predictive Control

TH Thermal Hydraulics

SPM Subcritical Power Module

CFD Computational Fluid Dynamics

SAM Systems Analysis Module

VHTR Very High Temperature Reactor

IQM improved quasi-static method

PCQM predictor-corrector quasi-static

1. INTRODUCTION

The overall aim of this project is to investigate and develop passive systems for semi-autonomous control of High Temperature Gas Reactor (HTGR) type Special Purpose Reactors (SPRs)—or microreactors. In previous work, we investigated the reactivity of the local temperature perturbation and variable reflector cross sections for passive control [3, 4], developed the simplified point kinetics model, and assessed the global and local reactivity for passive control systems [5]. Based on these investigations, we developed a MPC-based method using a state-space model that actively provided autonomous control of reactivity of a microreactor [6]. These investigations provided a reference for how well existing technologies will function given the task of reactivity control of a microreactor.

In this report, we continue our investigation by analyzing the feasibility of a passive reactivity control system. Investigating the feasibility of the variable flow controller for the load following is the first part of the work. These results help to determine the range of the power rate of the flexible power operation scenarios where the variable flow controller can be applied. Further, this analysis helps to characterize how the variable controller would need to operate for optimal control. These applicable operation conditions will be verified in future work with the high-fidelity simulation.

The second part of the work is to develop a simplified TH model for high-fidelity simulations. The TH model is very important since the passive control is based on the feedback from temperature. The hope is that a simplified TH model can provide reasonably accurate TH results and reduce the computational cost compared to the high-fidelity calculation from a Computational Fluid Dynamics (CFD) code or system code such as SAM [7, 1]. Another advantage is that the simplified model can be implemented directly in the neutron transport code PROTEUS [8] for this project. This helps to reduce the coding complexity of data transfer due to potential mesh inconsistencies between the neutronics code and the TH code. To verify the simplified TH model, the axial temperature distribution for a unit cell is calculated by the simplified TH model and compared to our previous SAM results.

The last part of the report is to lay out the plan for implementing and verifying the MPC capability in the PROTEUS code. The plan provides guidance on our future work in the project. To begin, we proceed with some background on the reactor design.

1.1 Holos Background

As a specific use case for an HTGR, we use the reactor design under development at Holos. The Holos-Quad design is a scaled down HTGR with the core being composed of four SPMs. Each SPM is effectively an independent closed-loop Brayton cycle power conversion unit with a nuclear heat source in a tube-shell heat exchanger configuration. This effectively eliminates the balance of plant. In earlier designs of this reactor, the four SPMs were configurable so that they will create a critical reactor. An illustration of the SPM is shown in Fig. 1.

The design has continued to evolve under the ARPA-E MEITNER program [9]. A new, proprietary design was developed by the ARPA-E Resource team at Argonne National Laboratory (ANL) and finalized on April 20th, 2020. The new design was reported in [10, 11]. The updated core design is the focus of the calculations and analysis of this report. The design with all drums in and out is pictured in Fig. 2. Since this time, the Holos reactor has gone through another iteration, and future work in the project may transition to this newest Gen 2+ design.

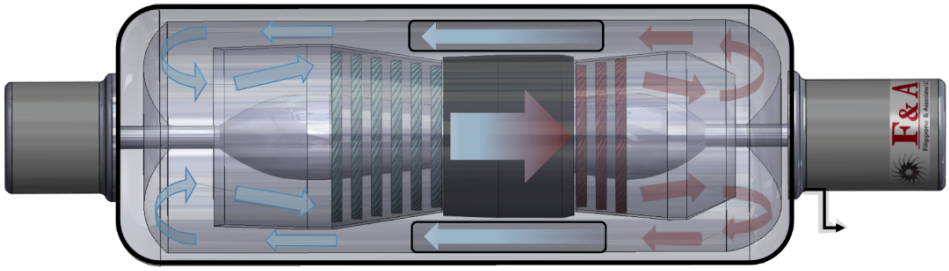

Figure 1. Illustration of an SPM.

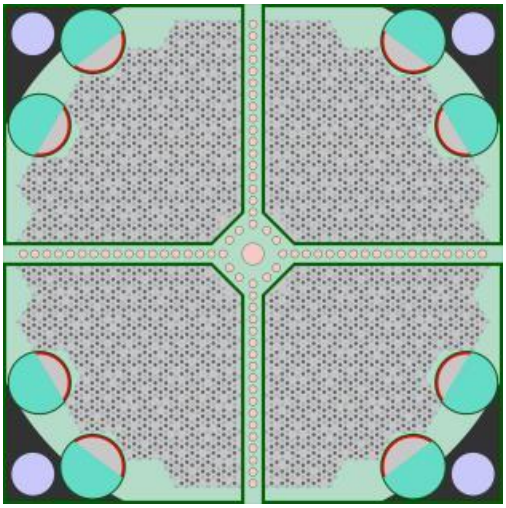

Figure 2. Preliminary Holos-Quad design with drum in.

1.2 Organization of this Report

The remainder of this report is organized as follows: first we present our methodology of analyzing the dynamics of the reactor and the MPC method for the control system. Next we present the results for studying the effect of varyiong the flow rate and preliminary control of the flow rate that a passive system would need to mimic. Then we present the development and verification of the simplified TH. Finally, we lay out the plan for the implementation of MPC.

2. SIMPLIFIED DYNAMICS MODEL AND MPC

In this section, we summarize the simplified dynamics model developed in previous investigations [5, 6]. The simplified model was used to verify the feasibility of the MPC that is the method adopted for development of the active control system using control drums. Therefore, the basis of MPC is also presented.

2.1 Simplified Reactor Dynamics Model

In our previous work, the point kinetics model coupled with feedback from a 3-temperature thermal-fluids model has been used as the simplified reactor dynamics model to assess the control algorithm in the Holos-quad reactor. In this document, these sets of equations are used to assess the performance of variable flow rate reactivity control on the evolution of the power.

2.1.1 Point Kinetics Model

The standard 6 delayed group point kinetics equations are used for the point-reactor model. These equations are given as:

$$\frac{dn(t)}{dt} = \frac{\rho(t) - \beta}{\Lambda} n(t) + \sum_{i=1}^{m} \lambda_i C_i(t)\,, \tag{1}$$

$$\frac{dC_i(t)}{dt} = \frac{\beta_i}{\Lambda} n(t) - \lambda_i C_i(t), \quad i = 1, 2, \ldots, m = 6\,, \tag{2}$$

where n is the neutron density, m is the number of delayed groups; ρ is the reactivity; β is the total effective neutron fraction; λ_i is the i-th group effective delayed neutron precursor decay constant; Λ is the generation time; and C_i is the i-th group precursor concentration.

The initial condition of the precursor concentration at steady-state is derived by setting the left side of Eq. (2) to be zero as follows:

$$C_{i0} = \frac{\beta_i n_0}{\lambda_i \Lambda}, \quad i = 1, 2, \ldots, m\,, \tag{3}$$

where the subscript 0 denotes the initial steady-state condition.

The point kinetics equations are normalized with the initial condition and are written as follows:

$$\frac{d\bar{n}(t)}{dt} = \frac{\rho(t) - \beta}{\Lambda} \bar{n}(t) + \sum_{i=1}^{m} \frac{\beta_i}{\Lambda} \bar{C}_i(t)\,, \tag{4}$$

$$\frac{d\bar{C}_i(t)}{dt} = \lambda_i \bar{n}(t) - \lambda_i \bar{C}_i(t), \quad i = 1, 2, \ldots, m\,, \tag{5}$$

where

$$\bar{n}(t) = \frac{n(t)}{n_0}\,, \tag{6a}$$

$$\bar{C}_i(t) = \frac{C_i(t)}{C_{i0}}\,. \tag{6b}$$

The non-dimensional normalized forms facilitate the expression for the temperature-feedback model and the derivation of the control system.

2.1.2 Three-temperature Thermal-Fluids Model

The equations for the 3-temperature thermal-fluids model are written as

$$m_f c_f \frac{dT_f(t)}{dt} = qP_r\bar{n}(t) - K_{fm}\left(T_f(t) - T_m(t)\right) , \tag{7}$$

$$m_m c_m \frac{dT_m(t)}{dt} = (1-q)P_r\bar{n}(t) + K_{fm}\left(T_f(t) - T_m(t)\right) - K_{mc}\left(T_m(t) - T_c(t)\right) , \tag{8}$$

$$m_c c_c \frac{dT_c(t)}{dt} = K_{mc}\left(T_m(t) - T_c(t)\right) - 2\dot{m}_c c_c\left(T_c(t) - T_{in}\right) , \tag{9}$$

where P_r is the rated power of the reactor; the dimensionless parameter q represents the fraction of heat deposited in the fuel (the rest being deposited in the moderator); m_f, m_m and m_c are the masses of the fuel, moderator, and coolant, respectively; $\dot{m}_c$ is the coolant flow rate; c_f, c_m and c_c are the heat capacities of the fuel, moderator, and coolant, respectively; K_{fm} and K_{mc} are the heat transfer coefficients from the fuel to moderator, and from the moderator to coolant, respectively; and T_{in} is the inlet coolant temperature. The equations are developed by treating the heat-balance of the fuel, moderator and coolant temperature separately.

The global heat transfer coefficients can be calculated directly based on their physical definitions with some approximation for the geometry. However, in our investigations [4, 6], we express the coefficients as

$$K_{fm} = \frac{qP_r}{T_{f0} - T_{m0}} , \tag{10}$$

$$K_{mc} = \frac{P_r}{T_{m0} - T_{c0}} , \tag{11}$$

where

$$T_{c0} = \frac{T_{in0} + T_{out0}}{2} , \tag{12}$$

is the nominal average coolant temperature.

2.1.3 Reactivity Feedback

The reactivity feedback model has the components for reactivity due to the control systems and passive feedback mechanisms. The Holos reactor has two ways to actively control reactivity. One is through the rotation of some combination of the control drums simultaneously. The other is by the shutdown rods located along the central reflector region and outside of the SPMs shell for emergency shutdown. In this model, only the reactivity from the control drums are considered.

The reactivity model with the control drum and various temperature feedback mechanisms is defined as follows:

$$\delta\rho(t) = \alpha_f \delta T_f(t) + \alpha_m \delta T_m(t) + \alpha_c \delta T_c(t) + \delta\rho_d(t) , \tag{13}$$

$$\frac{d\delta\rho_d(t)}{dt} = G_d^T Z_d(t) , \tag{14}$$

where $\delta\rho_d$ is the reactivity change due to the control system (drums); α_f is the temperature reactivity coefficient of fuel; α_m is the temperature reactivity coefficient of moderator; α_c is the temperature reactivity coefficient of coolant; and $\delta_f(t)$, $\delta T_m(t)$ and $\delta T_c(t)$ are the temperature changes of the

fuel, moderator, and coolant, respectively. G_d is the differential reactivity worth of the control drums; and Z_d is the velocity of the control drum.

The values of the kinetics parameter, coefficients in the thermal-fluid model, and the reactivity coefficients for the Holos reactor are listed in Table 1, and have been given in [4, 6].

Table 1. Coefficients of the Simplified Reactor Dynamics Model

Parameter	Value	Unit	Parameter	Value	Unit
β	480.10	pcm	α_f	-2.875	pcm/K
β_1	14.20	pcm	α_m	-3.696	pcm/K
β_2	92.40	pcm	α_c	0	pcm/K
β_3	78.00	pcm	c_f	977.00	J/kg/K
β_4	206.60	pcm	c_m	1697.00	J/kg/K
β_5	67.10	pcm	c_c	5188.60	J/kg/K
β_6	21.80	pcm	m_f	2002.00	kg
Λ	0.00168	s	m_m	11573.00	kg
λ_1	0.01270	1/s	m_c	500.00	kg
λ_2	0.03170	1/s	$\dot{m}_c$	17.50	kg/s
λ_3	0.11600	1/s	T_{f0}	1105.00	K
λ_4	0.31000	1/s	T_{m0}	1087.00	K
λ_5	1.40000	1/s	T_{in0}	864.00	K
λ_6	3.87000	1/s	T_{out0}	1106.00	K
n_0	2.25E+14	m^{-3}	K_{fm}	1.17E+06	W/K
P_r	22.00	MW	K_{mc}	2.16E+05	W/K
q	0.96	-			

2.1.4 Model with ^{135}Xe

^{135}Xe is not a critical factor in the control for a short time, however, in the daily load following operation, the ^{135}Xe build could be very important. The governing equations for xeon concentration are defined as:

$$\frac{dI(t)}{dt} = \gamma_I \Sigma_f v n_0 \bar{n}(t) - \lambda_I I(t)\,, \tag{15}$$

$$\frac{dX(t)}{dt} = \gamma_X \Sigma_f v n_0 \bar{n}(t) + \lambda_I I(t) - \lambda_X X(t) - \sigma_X v n_0 \bar{n}(t) X(t)\,, \tag{16}$$

where γ_I and γ_X are the fission yields of ^{135}I and ^{135}Xe, respectively; v is the average velocity of the thermal neutrons; λ_I and λ_X are the radioactive decay rates of ^{135}I and ^{135}Xe, respectively; and σ_X is the microscopic absorption cross section of ^{135}Xe.

After the xenon concentration is considered, the reactivity model from Eq. (13) is given by

$$\delta\rho(t) = \alpha_f \delta T_f(t) + \alpha_m \delta T_m(t) + \alpha_c \delta T_c(t) + \delta\rho_d(t) + \delta\rho_X(t)\,, \tag{17}$$

where $\delta\rho_X$ is the reactivity from ^{135}Xe.

2.2 Model Predictive Control

MPC is the principle algorithm we adopted for the control system. It is an advanced method to control a process [12]. Within the framework of MPC, the control inputs are computed for a relatively short time horizon in the future by evaluating a cost function. The cost function is defined in terms of the error between a desired set-point and predicted output, the actual cost of applying control variables, etc. The calculation of the control variables is repeated at each subsequent instant or time-window. The key feature of MPC is that it turns the control problem to an optimization problem.

In our previous reports, we focused on using a linear, time-invariant state-space model in [5, 6]. The basic theory of the MPC algorithm adopted in the previous work is summarized here. The model is developed by linearizing the simplified dynamics model presented in Section 2.1 at the steady-state, written as

$$\dot{\mathbf{x}}_\mathbf{c} = \mathbf{A}_\mathbf{c}\mathbf{x}_\mathbf{c} + \mathbf{B}_\mathbf{c}\mathbf{u}\,, \tag{18}$$

$$\mathbf{y}_c = \mathbf{C}_\mathbf{c}\mathbf{x}_\mathbf{c}\,, \tag{19}$$

where $\mathbf{x}$ is the state vector, $\mathbf{u}$ is the control vector, and $\mathbf{y}$ is the output vector. $\mathbf{A}_c$ is the system matrix, $\mathbf{B}_c$ is the input-to-state matrix and $\mathbf{C}_c$ is the state-to-output matrix.

The model is then discretized in time and written as:

$$\mathbf{x}_\mathbf{m}(k+1) = \mathbf{A}_\mathbf{m}\mathbf{x}_\mathbf{m}(k) + \mathbf{B}_\mathbf{m}\mathbf{u}(k)\,, \tag{20}$$

$$\mathbf{y}(k) = \mathbf{C}_\mathbf{m}\mathbf{x}_\mathbf{m}(k)\,, \tag{21}$$

where k is the time step index, $\mathbf{x}$ is the state vector, $\mathbf{u}$ is the control vector, and $\mathbf{y}$ is the output vector. The discretized system are typically obtained using numerical integration with the step size (or sampling interval) T_s.

Applying a finite difference approximation to Eq. (20) yields:

$$\mathbf{x}_\mathbf{m}(k+1) - \mathbf{x}_\mathbf{m}(k) = \mathbf{A}_\mathbf{m}\left(\mathbf{x}_\mathbf{m}(k) - \mathbf{x}_\mathbf{m}(k-1)\right) + \mathbf{B}_\mathbf{m}(\mathbf{u}(k) - \mathbf{u}(k-1))\,. \tag{22}$$

We make use of the following simplifying notation

$$\Delta(\cdot)(k) = (\cdot)(k) - (\cdot)(k-1)\,, \tag{23}$$

to yield

$$\Delta\mathbf{x}_\mathbf{m}(k+1) = \mathbf{A}_\mathbf{m}\Delta\mathbf{x}_\mathbf{m}(k) + \mathbf{B}_\mathbf{m}\Delta\mathbf{u}(k) \tag{24}$$

Note that the input to the state-space model is $\Delta\mathbf{u}_\mathbf{m}(k)$. The next step is to connect $\Delta\mathbf{x}_\mathbf{m}(k)$ to the output, $\mathbf{y}_\mathbf{m}(k)$. To do so, a new state variable vector is defined as

$$\mathbf{x}(k) = \begin{bmatrix} \Delta\mathbf{x}_\mathbf{m}(k)^T & \mathbf{y}(k) \end{bmatrix}^T \tag{25}$$

Note that

$$\begin{aligned} \mathbf{y}(k+1) - \mathbf{y}(k) &= \mathbf{C}_\mathbf{m}\left(\Delta\mathbf{x}_\mathbf{m}(k+1)\right) \\ &= \mathbf{C}_\mathbf{m}\mathbf{A}_\mathbf{m}\Delta\mathbf{x}_\mathbf{m}(k) + \mathbf{C}_\mathbf{m}\mathbf{B}_\mathbf{m}\Delta\mathbf{u}(k). \end{aligned} \tag{26}$$

Combining Eqs. (25) to (26) leads to the following discretized state-space model:

$$\overbrace{\begin{bmatrix}\Delta\mathbf{x_m}(k+1)\\ \mathbf{y}(k+1)\end{bmatrix}}^{\mathbf{x}(k+1)} = \overbrace{\begin{bmatrix}\mathbf{A_m} & \mathbf{o}_\mathbf{m}^T\\ \mathbf{C_m A_m} & 1\end{bmatrix}}^{\mathbf{A}}\overbrace{\begin{bmatrix}\Delta\mathbf{x_m}(k)\\ \mathbf{y}(k)\end{bmatrix}}^{\mathbf{x}(k)} + \overbrace{\begin{bmatrix}\mathbf{B_m}\\ \mathbf{C_m B_m}\end{bmatrix}}^{\mathbf{B}}\Delta\mathbf{u}(k)\,, \tag{27}$$

$$\mathbf{y}(k) = \overbrace{\begin{bmatrix}\mathbf{o}_\mathbf{m}^T & 1\end{bmatrix}}^{\mathbf{c}}\begin{bmatrix}\Delta\mathbf{x_m}(k)\\ \mathbf{y}(k)\,,\end{bmatrix} \tag{28}$$

called the augmented model, that will be used in the design of the predictive control. Assuming that at the sampling instant k_i, where $k_i > 0$, the state variable vector $\mathbf{x}(k_i)$ is available through measurement, then the state $\mathbf{x}(k_i)$ provides the current plant information. In reality, $\mathbf{x}(k_i)$ will contain noise, and this is neglected in the current state of our work. The future control trajectory is denoted by

$$\Delta\mathbf{u}(k_i)\,, \Delta\mathbf{u}(k_i+1)\,, \ldots, \Delta\mathbf{u}(k_i+N_c-1)\,, \tag{29}$$

where N_c is called the control horizon-dictating the number of parameters used to capture the future control trajectory. With the information given in $\mathbf{x}(k_i)$, the future state variables are predicted for N_p number of samples, where N_p is called the prediction horizon. N_p is also the length of the optimization window. We denote the future state variables as

$$\mathbf{x}(k_i \mid k_i)\,, \mathbf{x}(k_i+1 \mid k_i)\,, \ldots, \mathbf{x}\left(k_i+N_p \mid k_i\right) \tag{30}$$

where $\mathbf{x}(k_i+m \mid k_i)$ is the predicted state variable at k_i+m with given current plant information $\mathbf{x}(k_i)$. The control horizon N_c is chosen to be less than (or equal to) the prediction horizon N_p. It is possible to denote the state-space model for the prediction horizons as follows:

$$\mathbf{Y} = \mathbf{F}\mathbf{x}(k_i) + \mathbf{\Phi}\Delta\mathbf{U} \tag{31}$$

where

$$\mathbf{Y} = \begin{bmatrix}\mathbf{y}(k_i+1 \mid k_i) & \cdots & \mathbf{y}\left(k_i+N_p \mid k_i\right)\end{bmatrix}^T\,, \tag{32}$$

$$\Delta\mathbf{U} = \begin{bmatrix}\Delta\mathbf{u}(k_i) & \cdots & \Delta\mathbf{u}(k_i+N_c-1)\end{bmatrix}^T\,, \tag{33}$$

$$\mathbf{F} = \begin{bmatrix}\mathbf{CA}\\ \vdots\\ \mathbf{CA}^{N_p}\end{bmatrix}\,, \tag{34}$$

$$\mathbf{\Phi} = \begin{bmatrix}\mathbf{CB} & 0 & 0 & \cdots & 0\\ \mathbf{CAB} & \mathbf{CB} & 0 & \cdots & 0\\ \mathbf{CA}^2\mathbf{B} & \mathbf{CAB} & \mathbf{CB} & \cdots & 0\\ \vdots & & & & \\ \mathbf{CA}^{N_p-1}\mathbf{B} & \mathbf{CA}^{N_p-2}\mathbf{B} & \mathbf{CA}^{N_p-3}\mathbf{B} & \cdots & \mathbf{CA}^{N_p-N_c}\mathbf{B}\end{bmatrix}\,. \tag{35}$$

For a given set-point signal (or reference trajectory), the objective of the predictive control system is to make the cost function as small as possible. It is assumed that the set-point signal remains constant in the optimization window. This objective is then translated into an input to find the

"best" control parameter vector $\Delta\mathbf{U}$ such that cost function is minimized with the cost function J defined as follows:

$$J(\Delta\mathbf{U}) = (\mathbf{R_s} - \mathbf{Y})^T \mathbf{Q} (\mathbf{R_s} - \mathbf{Y}) + \Delta\mathbf{U}^T \overline{\mathbf{R}} \Delta\mathbf{U} \tag{36}$$

where the data vector $\mathbf{R}_s^T$ contains the set-point information $r(k_i)$ as follows:

$$\mathbf{R}_s^T = \overline{\mathbf{R}}_\mathbf{s} r(k_i) = \overbrace{\begin{bmatrix} 1 & 1 & \cdots & 1 \end{bmatrix}}^{N_p} r(k_i) \tag{37}$$

In Eq. (36), the first term is linked to the objective of minimizing the errors between the predicted output $\mathbf{Y}$ and the set-point signal $\mathbf{R_s}$. The second term reflects the consideration given to the size of $\Delta\mathbf{U}$ when the objective function J is made to be as small as possible. $\overline{\mathbf{Q}}$ is a diagonal matrix in the form that $\overline{\mathbf{Q}} \in \mathbb{R}^{N_p \times N_p}$. It represents the weight of the error in each step. For most of our investigations Q is the identity matrix so that the error of each step in the prediction horizon has the same importance. $\overline{\mathbf{R}}$ is a diagonal matrix in the form that $\overline{\mathbf{R}} \in \mathbb{R}^{N_c \times N_c}$. It is used as a tuning parameter for the desired-loop performance. It can also be considered as the cost of changing a control input. Minimizing the cost function defined in Eq. (36) is an optimization problem, and is written as

$$\begin{array}{ll} \min_{\Delta\mathbf{U}} & J(\Delta\mathbf{U}) \\ \text{s.t.} & u_{\min} \le u_k \le u_{\max}, k = 0, \ldots, N_c - 1 \\ & y_{\min} \le y_k \le y_{\max}, k = 1, \ldots, N_p \\ & \Delta u_{\min} \le \Delta u_k \le \Delta u_{\max}, k = 0, \ldots, N_c - 1 \\ & \cdots \text{(other constraints)} \end{array} \tag{38}$$

Here the constraints are introduced. More details can be found in [6]. Algorithms developed from the field of convex optimization [13] can be used to solve these problems.

3. EFFECT OF THE VARIABLE FLOW RATE

Using the simplified reactor dynamics model to investigate the effect of the variable flow rate helps to provide insights into the passive control system prior to using the high-fidelity code for a more thorough analysis.

3.1 Ramp Flow Rate Change

In this study, it is assumed that the coolant flow rate is reduced from 100% $\dot{m}_{c0}$ at 0 s to 30% $\dot{m}_{c0}$ at a fixed speed r, where $\dot{m}_{c0}$ stands for the full power steady-state coolant flow rate. The rs investigated are 1% $\dot{m}_{c0}$/s, 2% $\dot{m}_{c0}$/s and 10% $\dot{m}_{c0}$/s.

The implicit assumption used in these calculations is that the change of the flow rate does not change the total mass of coolant inside the core. Therefore, in these simulations, m_c is a constant.

The results are shown in Fig. 3. It can be seen that reducing the coolant flow rate does reduce the total power. Therefore, changing the flow rate can provide passive control for the power. The power of all the cases eventually reaches the same asymptotic level that is around 46 %. Therefore, the passive control system should only work in certain power ranges for the load following.

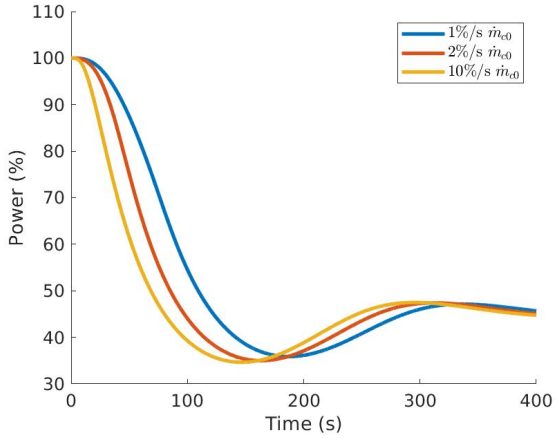

(a) Evolution of power

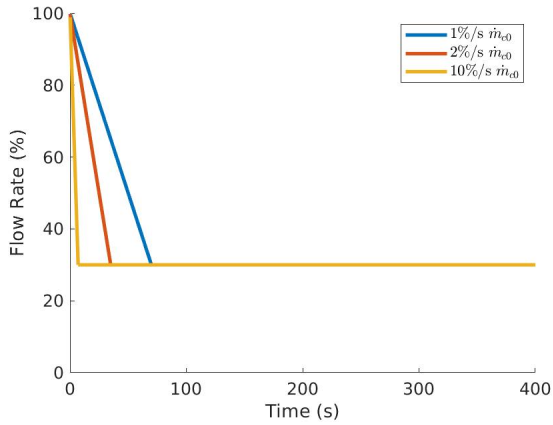

(b) Evolution of coolant flow rate

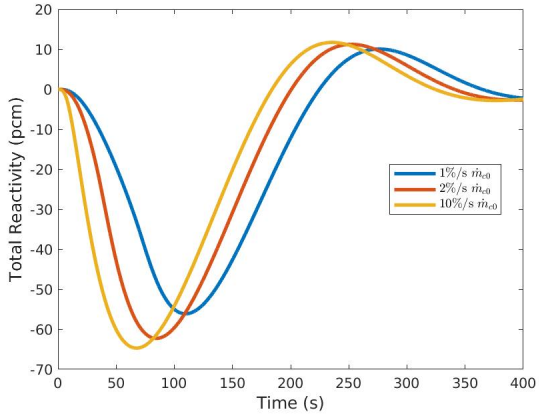

(c) Evolution of total reactivity

Figure 3. Results with variable coolant flow rate

It could also be observed that the magnitude of the maximum inserted reactivity is smaller than 65 pcm. In our previous work we estimated that a 33% change in flow rate could give up to a 380 pcm reactivity insertion. So, we see that these initial rough estimates were much larger than what might be realized with the simplified dynamics. The reactivity eventually returns to 0 pcm due to the feedback from the fuel and moderator. In the previous work [5], it has been shown that the control drums can insert more than 3000 pcm of reactivity. Therefore, compared to the control drum, it could be expected that the control capability of the passive control system with variable flow rate is much more limited.

Compared to the instantaneous reactivity insertion from the control drum rotation, it takes much longer time for the reactivity from temperature feedback becomes dominant. For the 10% $\dot{m}_{c0}$/s case, the flow rate reaches the set point 30% $\dot{m}_{c0}$ at 7 s. The reactivity, however, reaches its maximum in magnitude around 50 s. The reason is that the reactivity insertion is due to the variation of the temperature, while the variation of temperature is determined by the heat capacity and heat transfer coefficients primarily of the graphite. Therefore, the control system based on a variable flow rate can be considered as a system with delay.

3.2 Step Flow Rate Change

Fig. 4 compares the evolution of the reactivity with the control drum position or the flow rate perturbed significantly at the start time. In one case, the group A control drums are rotated by 4°, and in the other, the variable flow rate is set to 30% $\dot{m}_{c_0}$. It should be noted the transient is impractical in that the flow rate could not change this fast. Therefore, it is only used to show the response of the reactivity to the control system. Both cases have similar minimum reactivity. Once again, it is observed that the response of the reactivity to the flow rate change is much slower than the drum position.

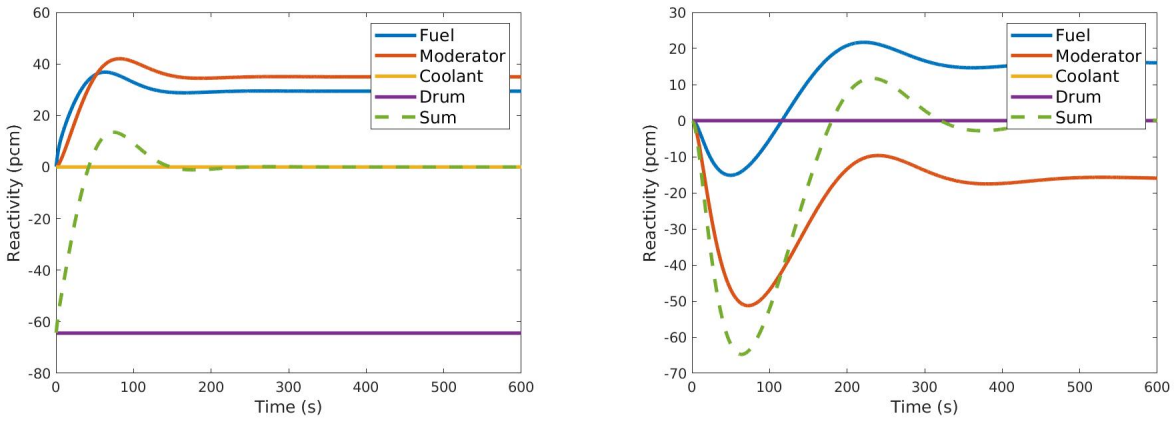

(a) Reactivity inserted by step control drum position change

(b) Reactivity inserted from step variable flow rate change

Figure 4. Reactivity as the function of time with control variables perturbed at the start time

Therefore, it could be expected that a passive control system based on a variable flow rate may only be used in the load follow with small power ramp rates. In the case with fast power change, the reactivity from the control variable should be inserted instantaneously. The passive control system however cannot insert substantial reactivity promptly.

3.3 Effect on the Model Predictive Control

In this section, the performance of the system using a MPC controller to change the flow rate is illustrated. These calculations help to characterize how the passive system should behave. The plant model is the simplified reactor dynamics model. The model used in the MPC controller is the state-space model from linearizing the dynamics model at the steady-state.

For the passive controller, the state vector (neglecting the drum position) is

$$\mathbf{x_c} = \left[\delta\bar{n}(t) \quad \delta\bar{C}_1(t) \quad \cdots \quad \delta\bar{C}_m(t) \quad \delta T_f(t) \quad \delta T_m(t) \quad \delta T_c(t) \quad \delta\dot{m}_c(t)\right]^T . \tag{39}$$

Here we use the definition,

$$\delta(\cdot)(t) = (\cdot)(t) - (\cdot)(0) . \tag{40}$$

$\mathbf{A_c}$ is expressed as:

$$\mathbf{A_c} = \begin{bmatrix} -\frac{\beta}{\Lambda} & \frac{\beta_1}{\Lambda} & \cdots & \frac{\beta_m}{\Lambda} & \frac{\alpha_f}{\Lambda} & \frac{\alpha_m}{\Lambda} & \frac{\alpha_c}{\Lambda} & 0 \\ \lambda_1 & -\lambda_1 & \cdots & 0 & 0 & 0 & 0 & 0 \\ \vdots & \vdots & \vdots & \vdots & \vdots & \vdots & \vdots & \vdots \\ \lambda_m & 0 & \cdots & -\lambda_m & 0 & 0 & 0 & 0 \\ \frac{qP_r}{m_f} & 0 & \cdots & 0 & -\frac{K_{fm}}{m_f c_f} & \frac{K_{fm}}{m_f} & 0 & 0 \\ \frac{(1-q)P_r}{m_m c_m} & 0 & \cdots & 0 & \frac{K'_{fm}}{m_m c_m} & -\frac{K'_{mm}}{m_m c_m} & \frac{K_{mc}}{m_m c_m} & 0 \\ 0 & 0 & \cdots & 0 & 0 & \frac{K_{mc}}{m_c c_c} & -\frac{K_{mc}c+2\dot{m}_c c_c}{m_c c_c} & -\frac{2(T_{c0}-T_{in})}{m_c} \\ 0 & 0 & \cdots & 0 & 0 & 0 & 0 & 0 \end{bmatrix}, \tag{41}$$

$\mathbf{B}_c$ is

$$\mathbf{B_c} = \begin{bmatrix} 0 & 0 & \cdots & 0 & 0 & 0 & 0 & 1 \end{bmatrix}^T, \tag{42}$$

The control vector is

$$\mathbf{u} = [r(t)], \tag{43}$$

and the output vector is

$$\mathbf{y} = \left[\delta\bar{n}(t)\right]. \tag{44}$$

In this part, the weight matrix for the tracking error $\mathbf{Q}$, and the weight matrix for the cost of applying the control variable in Eq. (36) are defined by

$$\mathbf{Q} = \mathbf{I}_{N_p \times N_p}, \tag{45}$$

$$\bar{\mathbf{R}} = R_w ||\mathbf{\Phi}^T \mathbf{\Phi}|| \mathbf{I}_{N_c \times N_c}. \tag{46}$$

$\bar{\mathbf{R}}$ is defined in terms of the norm $||\mathbf{\Phi}^T \mathbf{\Phi}||$ so that a better balance of the cost of the tracking error and control variable are achieved.

As investigated in the previous section, the passive controller with flow rate is a delayed control system. In this case, the weight matrix $\bar{\mathbf{R}}$ is very important so that the optimization problem in Eq. (38) has a unique solution [14]. The range of prediction horizon is also very important. N_p must be large enough so that the effect of the control variables can be captured.

3.4 Effect of Prediction Horizon and Weight R_w

The test case used in this part has a power change rate set-point of 10% P_0/min. The minimum power is 60%P_0. The sampling interval (or the step size) T_s is 0.1 s. We are aware that the sampling interval may not be the real value used in the control system adopted in the reactor field. The results shown here are simply used assess passive controller with MPC and show the effect of the prediction horizon and weight R_w.

Fig. 5 shows the evolution of the power with the prediction horizon $N_p = 10$. It can be seen that whatever weight matrix is used, the passive controller cannot let the power track the set-point very well.

Fig. 6 shows the evolution of the power, error of the power and flow rate for the passive controller with the prediction horizon $N_p = 30$ and the weight $Rw = 5 \times 10^{-5}$. Now it can be found that

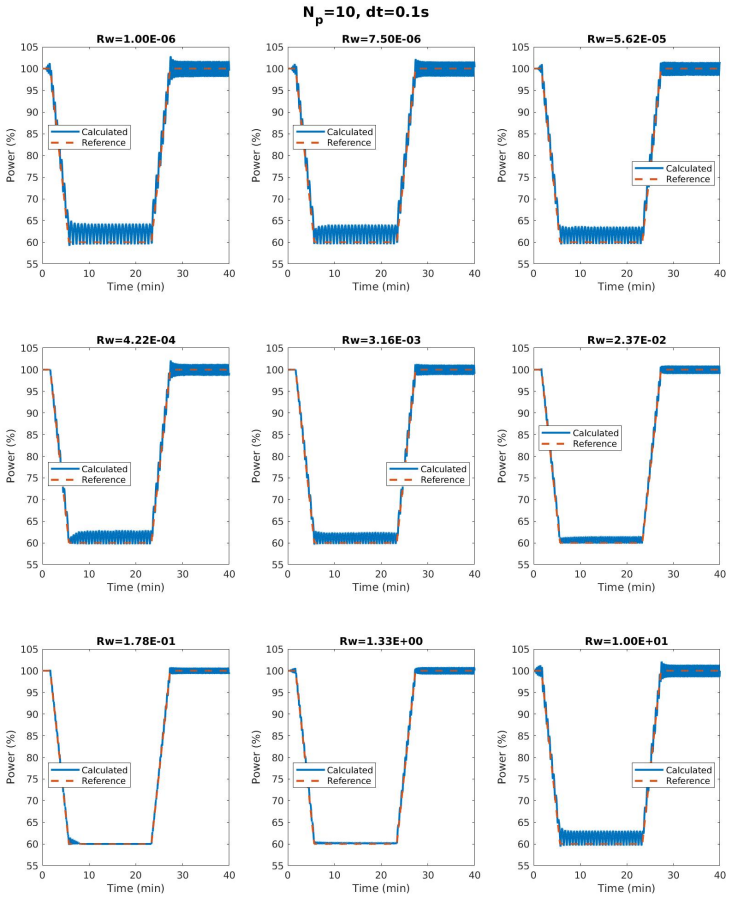

Figure 5. Effect of Rw on the evolution of the power with $N_p = 10$ for 10% P_0/min.

the MPC can achieve relatively good agreement between the real power and the set-point power. However the flow rate oscillates in a very wide range. In fact, for all the applicable Rw, the flow rate oscillates significantly. So even though the MPC can compute a control solution, it is not feasible. This is impractical because the mechanical system could not change the flow rate as fast as the model predicted.

When $N_p = 60$, the flow rate varies more smoothly as suggested in Fig. 7. The magnitude of the tracking error is much smaller. However, the flow rate must be changed very fast at the region where the reference power stops changing or starts changing.

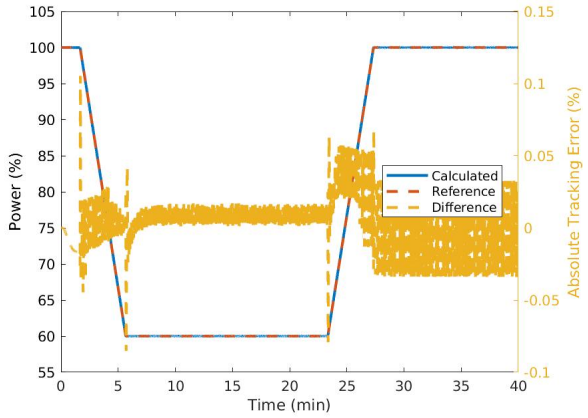

(a) Evolution and error of the power

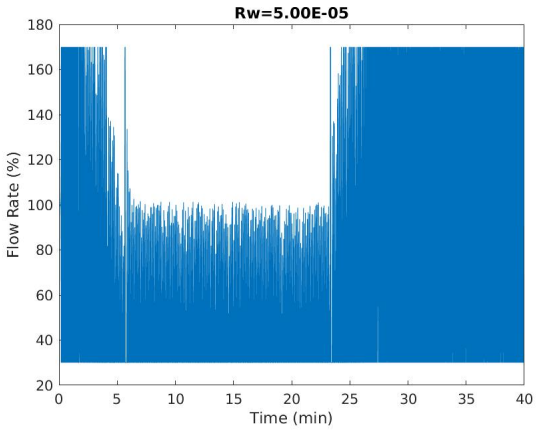

(b) Evolution flow rate

Figure 6. Evolution of the power, error of power, flow rate for controller with $N_p = 30$ and $R_w = 5 \times 10^{-5}$ for 10% P_0/min.

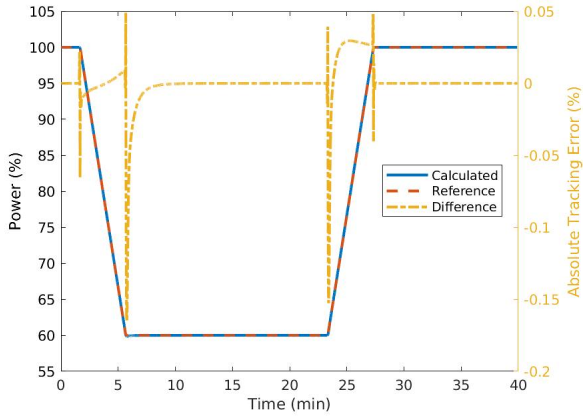

(a) Evolution and error of the power.

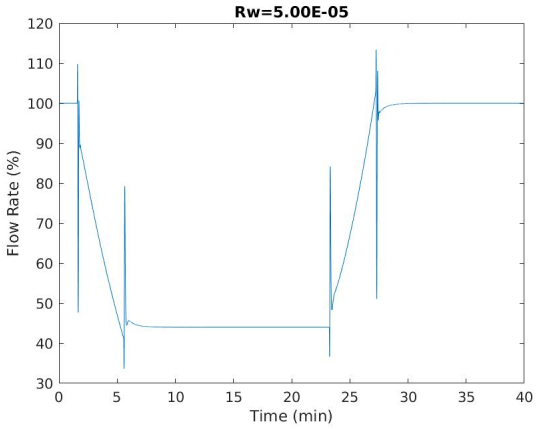

(b) Flow rate

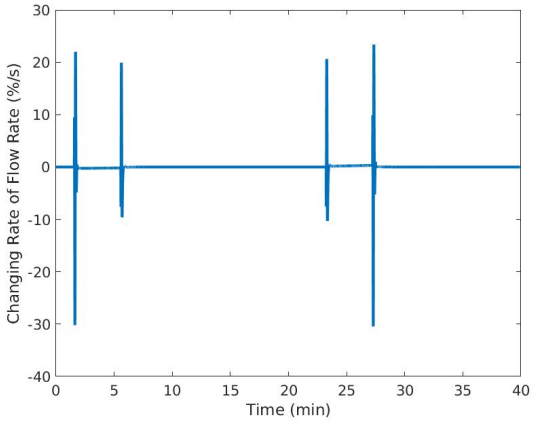

(c) Change rate of Flow Rate

Figure 7. Results for passive controller with $N_p = 60$ and $R_w = 5 \times 10^{-5}$ for 10% P_0/min.

3.5 Small Ramp Rate Cases

As illustrated above, the 10% P_0/min ramp rate for power set-point is hard to achieve for controller with flow rate. Here, we show that the passive control can be better applied to cases with a smaller power change rate. From Figs 8, it can be observed that the flow rate controller can let the power follow the trajectory very well. The smaller the power change rate is, the smaller the tracking error is. For the case with a power change rate of 5% P_0/min, the maximum error is less than 0.1%P_0. However, a larger flow rate change is required when the power changes. For the case with 5% P_0/min change, the flow rate must be as large as 15% $\dot{m}_{c0}$/s. This may possess some challenges for the passive control system.

To summarize, in this part, we have shown that the MPC method can compute control responses that a passive system would need to possess to achieve passive control with flow rate for load following. Compared to using drum controller, the passive control is harder. The success of the passive controller in the simplified dynamics problem lies in that the prediction horizon must be long enough. The reason is that the passive control by flow rate is a delayed control system. The MPC can let the tracking error be smaller than 0.1% P_0 for cases with power change rate smaller than 5% P_0/min. However, the "big-bang" nature of the control actions are likely not easily achieved by a passive system.

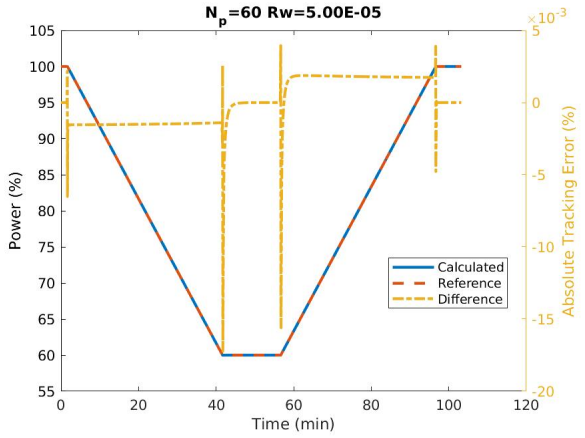

(a) Evolution and error of the power for 1% P_0/min

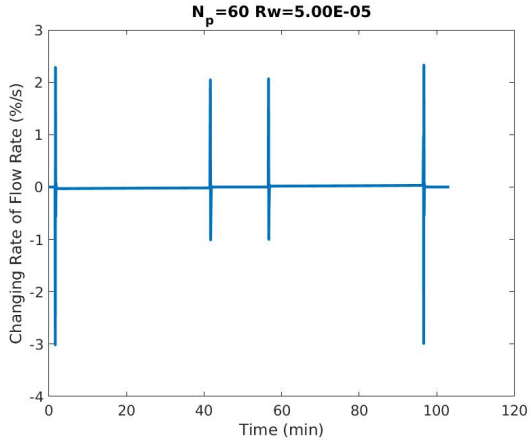

(b) Change rate of flow rate for 2% P_0/min

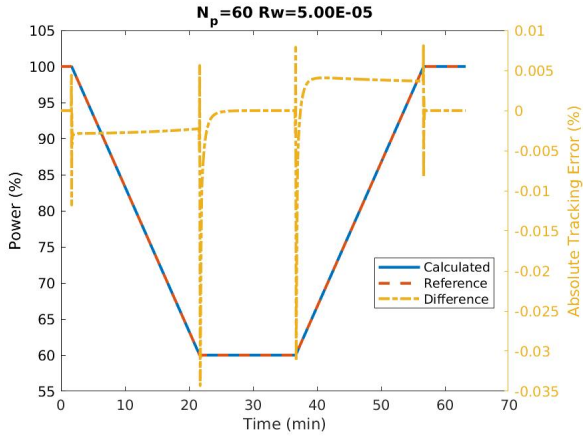

(c) Evolution and error of the power for 2% P_0/min

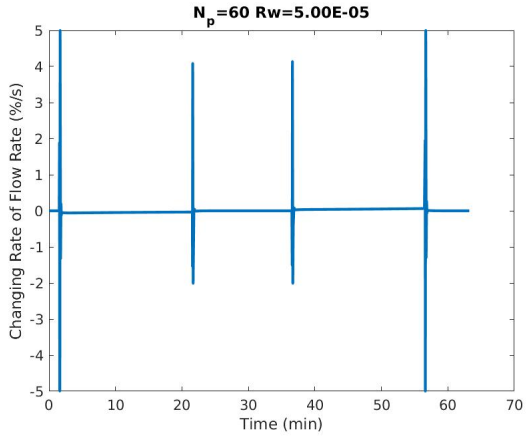

(d) Change rate of flow rate for 2% P_0/min

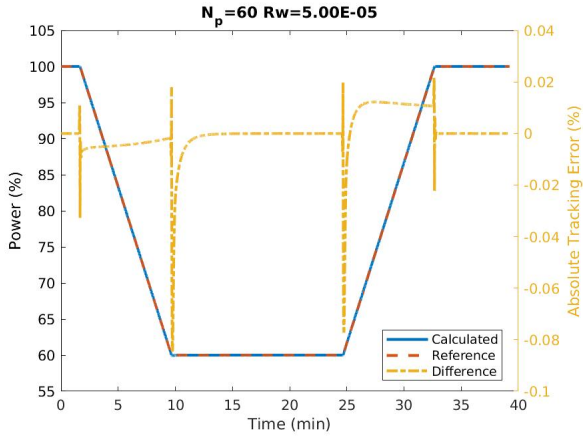

(e) Evolution and error of the power for 5% P_0/min

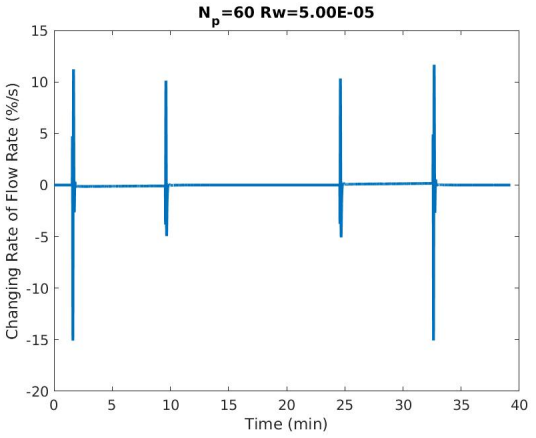

(f) Change rate of flow rate for 5% P_0/min

Figure 8. Results for passive controller with $N_p = 60$ and $R_w = 5 \times 10^{-5}$ for cases with small power change rate.

4. VERIFICATION AND IMPLEMENTATION PLAN OF THE SIMPLIFIED TH MODEL

The applicability of the controller and its underlying simplified dynamics model will be assessed with high-fidelity multiphysics simulations in future work. Presently, simplified TH model is developed for the solution of the TH problem and implementation of a control algorithms in PROTEUS. The simplified model is developed based on the model proposed in [1]. The model has been validated for VHTR designs and can predict the fuel temperature quite well (frequently within a few degrees C compared to CFD results). Compared to the TH calculation with advanced tools such as the SAM code or CFD codes, the computational cost of the simplified TH is much less. This is our primary motivation for adopting this model, as we begin to explore the dynamics with PROTEUS.

4.1 Simplified TH Model for VHTR

We propose that the simplified TH model for the VHTR model is appropriate for the Holos design since the heat transfer characteristics are very similar to VHTR designs. The illustration of the simplified TH model for the VHTR unit cell is shown in Fig. 9. The equations are given by:

$$T_{gc} = T_c + \frac{q''_s}{h_c}, \tag{47a}$$

$$T_{gf} = T_{gc} + \frac{2A_g}{P_f + P_c}\frac{q''_s}{k_g}, \tag{47b}$$

$$T_{fs} = T_{gf} + \frac{q''_s}{h_g}, \tag{47c}$$

$$T_{fc} = T_{fs} + \frac{r_f}{2}\frac{q''_s}{k_f}, \tag{47d}$$

where q''_s is the heat flux at the fuel compact surface; T_c is the bulk coolant temperature; h_c and h_g are heat transfer coefficient at coolant hole surface and fuel compact gap, respectively; r_f is the radius of fuel compact; A_g is the area of graphite block of the unit cell model; P_f and P_c are arc length of fuel compact and coolant channel of the unit cell model; k_f and k_g are the heat conduction coefficient of fuel compact and graphite block, respectively.

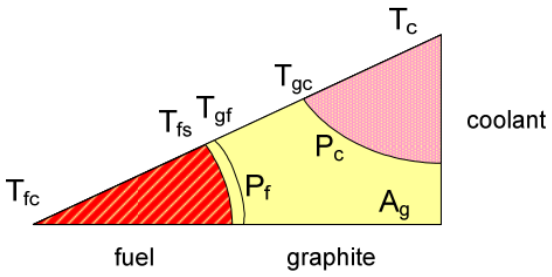

Figure 9. Simplified unit cell TH model for VHTR [1].

The average fuel and graphite temperature are then determined as weighted averages of T_{fc}, T_{fs},

T_{gc} and T_{gf} as:

$$\bar{T}_f = \left(1 - w_f\right) T_{fc} + w_f T_{fs} \tag{48}$$

$$\bar{T}_g = \left(1 - w_g\right) T_{gc} + w_g T_{gf} \tag{49}$$

where T_{fc} is fuel center line temperature; T_{fs} is fuel surface temperature; T_{gf} is graphite temperature at the interface with fuel, T_{gc} is graphite temperature at the interface with coolant.

The coefficients k_f, k_g are specified by users and w_f and w_g are problem-dependent. It is expected that the values of these coefficients provided by [1] may not provide reasonably accurate results for modeling Holos design.

4.2 Simplified TH Model for Holos Design

The simplified TH model in Eq. (47) however must be modified slightly to be consistent with Holos design and the SAM model used in [3].

The simplified unit cell TH model of the Holos design is shown in Fig. 10. Compared to the

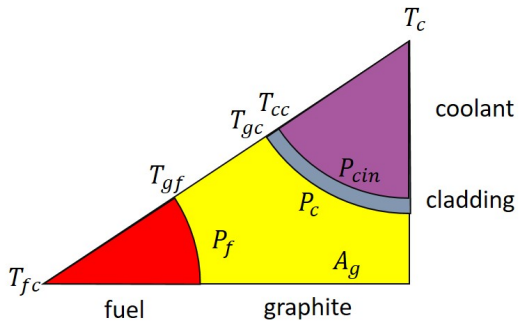

Figure 10. Simplified unit cell TH model for Holos design.

VHTR model, one modification is that a cladding is present around the coolant channel. The other modification is that h_g is assumed to be infinity, e.g there is no thermal resistance between the compact and block. The graphite cross sectional area is

$$A_g = \frac{S_A - n_c A_c - n_p A_p}{n_f} - A_f \tag{50}$$

where S_A is the cross sectional area of the assembly; A_c is the area of the coolant and the cladding; A_p and A_f are the area of the poison and fuel compact, respectively; n_p is the number of poison rods; n_c and n_f are the number of coolant channels and the number of fuel compacts per assembly, respectively. The heat transfer coefficient h_c between the coolant and the cladding is obtained with the Dittus-Boelter correlation [15]:

$$Nu = 0.023 Re^{0.4} Pr^{0.8}\,. \tag{51}$$

The equations for the new simplified TH model are then expressed as:

$$T_{cc} = T_c + \frac{q''_f}{h_c}\frac{P_f n_f}{P_c n_c}, \tag{52a}$$

$$T_{gc} = T_{cc} + \frac{q''_f P_f}{2\pi k_{cd}}\frac{n_f}{n_c}\ln\frac{P_c}{P_{cin}}, \tag{52b}$$

$$T_{gf} = T_{gc} + \frac{2A_g}{P_f + P_c}\frac{q''_s}{k_g}, \tag{52c}$$

$$T_{fs} = T_{gf}, \tag{52d}$$

$$T_{fc} = T_{fs} + \frac{r_f}{2}\frac{q''_s}{k_f}, \tag{52e}$$

where T_{cc} is the cladding temperature at the interface with coolant; k_{cd} is defined as the heat conduction coefficient for the cladding.

For the steady state calculation, the bulk temperature of the coolant is calculated first by conservation of energy using

$$T_c(h) = T_{in} + \frac{1}{C_{p,c}\dot{m}_{c0}}\int_0^h \frac{q''_l(s)P_f n_f}{n_c}ds, \tag{53}$$

where $C_{p,c}$ is the specific heat capacity of the coolant. Then the temperature of cladding, graphite and fuel is calculated using Eq. (52). Once the temperature at the interface is obtained, the averaged cladding temperature is then defined by

$$T_{clad} = \frac{T_{cc} + T_{gc}}{2}. \tag{54}$$

For the transient calculation, the sequence of calculations is reversed from the steady-state calculation. The fuel temperature is updated first by solving

$$\rho c_p \frac{\partial T}{\partial t} = \nabla \cdot k\nabla T + q''', \tag{55}$$

with the steady-state solution as the initial condition. Then the graphite, cladding,and coolant temperatures are updated with the simplified model. Verification of the transient calculation from coupling the PROTEUS and the simplified model will be the topics of the future reports.

4.3 Numerical Verification

In this part, we compare the simplified TH calculation results with the SAM results that have been presented in [3]. The calculation is performed for a unit cell. The power distribution is predefined and shown in Fig. 11.

The parameters used for the SAM model are summarized in Table 2 and are also used in the simplified model. The thermal properties of the coolant are calculated using the expressions from

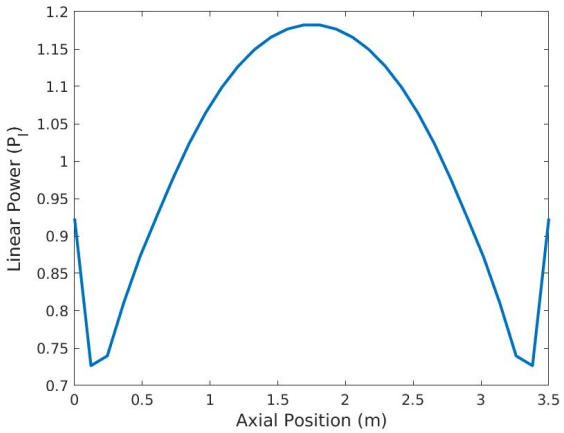

Figure 11. Predefined axial Power distribution.

Table 2. Parameters involved in TH calculation.

Parameter	Value	Unit	Parameter
Averaged Power	P	2.5397	kW/m
Height	H	3.5	m
Coolant Inlet Parameter	T_{in}	590.0	C
Pressure	p	7	MPa
Coolant Inlet Velocity	V	29.9	m/s
heat conduction coefficient of graphite	k_g	30	J/m· K
heat conduction coefficient of fuel	k_g	18	J/m· K

[16] with the inlet temperature, velocity and pressure. The w_g and w_f are the same as those used in [1].

The plots of averaged cladding temperature and fuel temperature are shown in Fig. 12. It can be seen that the temperature distributions calculated by the simplified TH model agree well with the SAM results.

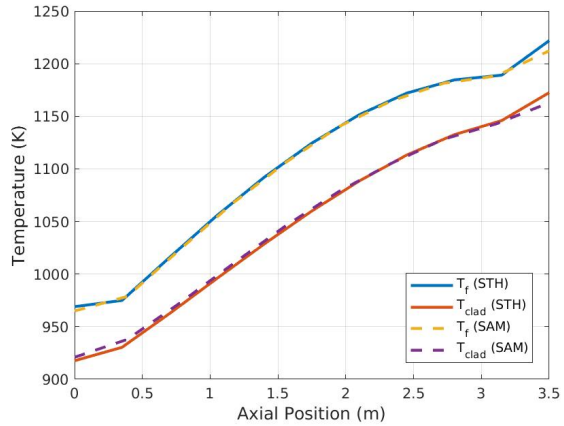

Figure 12. Axial temperature distribution. "STH" stands for simplified TH.

4.4 Implementation Plan for Coupling Calculation

In the steady-state calculation, the PROTEUS is coupled with TH feedback via Picard iteration. The specific algorithm adopted will be the Picard iteration scheme analyzed in [2].

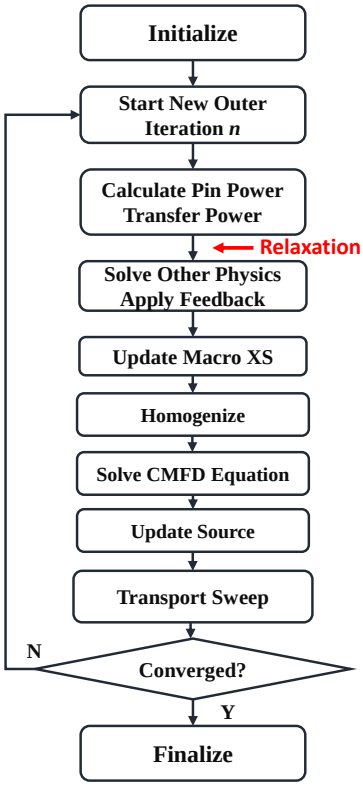

Figure 13. Proposed Picard iteration scheme to couple the PROTEUS and simplified TH model for steady-state problem [2].

With this iteration scheme, the transport problem is only solved partially by PROTEUS every source iteration. This not only helps to reduce the computation cost of the neutronics calculation per iteration, but also improves the convergence rate of the solution. Since the Holos reactor is a small-sized problem, we expect the instability issue should not be confronted.

For the transient calculation, the operator splitting will be used for the coupling. The algorithm should be the same as what has been used to couple PROTEUS and SAM in [17].

5. IMPLEMENTATION PLAN OF MODEL PREDICTIVE CONTROL IN PROTEUS

In this section, we will introduce how we are going to implement the model predictive control capability in PROTEUS to support the verification of the MPC model.

5.1 State-Space Model

The state-space model is derived based on the point kinetics equations. We desire the parameters used for point kinetics model to characterize the dynamics of the high-fidelity model. The best we can hope to do do with simulation is to obtain the real-time point kinetics equations and feedback models from the high-fidelity simulation, and then derive the state-space model. We denote this as the real-time model. The MPC control we have demonstrated so far has usedonly predefined parameters. A key question in the MPC is: how accurate the model used by MPC needs to be? This is one main research question we wish to answer in this project. Therefore, we also suggeset to establish a predefined point-kinetics model coupled with a TH model embedded in PROTEUS for comparison. The plan for the development of these models is described.

5.1.1 Real-time Model

The real-time model can be developed since the improved quasi-static method (IQM) and predictor-corrector quasi-static (PCQM) have been implemented in PROTEUS recently [18]. The basis of these two solvers is to construct the equivalent point kinetics models, and use the point kinetics solution to correct the transport solution.

Therefore, during the high-fidelity simulation, the point kinetics parameters are already computed, stored, and used. We will simply reuse these parameters at each PROTEUS time step to obtain the latest point kinetics model from which we will construct the state-space model for the MPC controller. Additionally, tor the feedback model, the averaged temperature can be computed, and the relation between the temperature and reactivity can be obtained via on-the-fly regression. This will complete the required information for the state-space model.

Once the latest state-space model is defined, the MPC controller will be run to compute the control action on the control variable for the next time step of the high-fidelity simulation. The control variable will then introduce a new perturbation to the transient simulation, and the time-dependent high-fidelity simulation continues with the new perturbation computed by the MPC controller. If the models obtained are very accurate, then the real-time model will likely represent the best the MPC can achieve and provide a reference for offline models.

5.1.2 Predefined Model

Using the predefined model for the MPC calculations is more practical, and the traditional way of utilizing MPC control. It is proposed here that we will use the high-fidelity time-dependent simulations to obtain parameters for the point kinetics model and the feedback model needed by the MPC calculation by running a few step reactivity change transients. Then this model will be run offline to predict the dynamic response of the reactor for a given power maneuver. The model in this MPC calculation would remain unchanged during the whole simulation of the power maneuver. Thus, this model is obtained before using the high-fidelity simulation to verify the autonomous control. Ultimately, we hope to show that this approach is feasible for autonomous control.

5.1.3 Sensitivity Study

So far, the point kinetics parameters are obtained from the high-fidelity simulation as a stand-in for the actual physical plant model. In practical operation, however, the plant model however is the plant itself. To investigate the robustness of the MPC in the practical operation, a sensitivity study is necessary and will also be conducted in future work.

5.2 Nonlinear MPC

The model used for MPC so far is the linear time-invariant model that is linearized around the equilibrium state. The linear-invariant model is then discretized in time to provide the state-space model and the operators $\mathbf{A}_m$, $\mathbf{B}_m$, and $\mathbf{C}_m$ are assumed to be constant. However, as illustrated in Section 2.1, the dynamics model is nonlinear. The operators A_c and B_c should be updated at each time point in the discretized state-space model. When the perturbation introduced by the control variable is small, and the state variable is close the the initial state, use of a constant A_c and B_c will not degrade the performance of controller. When a state variable is far from the initial state, however, the nonlinearity will make the problem much harder and the model less consistent. It is expected that when the magnitude of the reactivity inserted by the control drum is large, the the time-invariant treatment of the state-space model will not be suitable. Further, in the passive control, the reactivity is introduced by a perturbation of the temperature. Therefore, it is also expected that using a nonlinear model in the model-based control should improve the performance of the passive control.

The MPC based on the nonlinear model is called nonlinear MPC [19]. In nonlinear MPC, the model is given by

$$\dot{\mathbf{x}}(t) = \mathbf{A}(\mathbf{x}, t, \mathbf{u})_c \mathbf{x}(t) + \mathbf{B}(\mathbf{x}, \mathbf{u}, t)_c \mathbf{u}(t) \tag{56}$$

Eq. (20) at k_{th} prediction of time t turns to be

$$\mathbf{x_m}(k+1) = \mathbf{A_m}(k)\mathbf{x_m}(k) + \mathbf{B_m}(k)\mathbf{u}(k)\,. \tag{57}$$

where $\mathbf{A_m}(k)$ and $\mathbf{B_m}(k)$ are obtained at $t+T_s k$, and T_s is the sampling interval. Now both operators are obtained with the latest state variables and vary in time.

The optimization problem for the nonlinear representation then becomes

$$\begin{aligned} \min_{\mathbf{\Delta U}} J(\Delta \mathbf{U}) &= (\mathbf{R_s} - \mathbf{Y})^T \mathbf{Q} (\mathbf{R_s} - \mathbf{Y}) + \Delta \mathbf{U}^T \overline{\mathbf{R}} \Delta \mathbf{U} \\ \text{s.t. } & \mathbf{x_m}(k+1) = \mathbf{A_m}(k)\mathbf{x_m}(k) + \mathbf{B_m}(k)\mathbf{u}(k) \\ & y_{\min} \le y_k \le y_{\max}, k = 1, \ldots, N_p \\ & \Delta u_{\min} \le \Delta u_k \le \Delta u_{\max}, k = 0, \ldots, N_c - 1 \\ & \cdots \text{(other constraints)} \end{aligned} \tag{58}$$

This optimization problem is generally nonlinear, therefore nonlinear optimization methods are required. Additionally, the solutions are typically only locally optimal. More details on the nonlinear MPC will be covered in the next report.

5.3 Basic Solvers

To implement the aforementioned MPC controllers in PROTEUS, some basic solvers are necessary. These solvers include

- Continuous model to discretized model solver. This solver will convert the continuous model Eq. (18) to the discretized model Eq. (20).
- Quadratic programming solver. For the MPC with constant operators, the optimization problem is a quadratic programming problem. The quadratic programming solver will be implemented to solve this problem.

- Nonlinear programming solver. When nonlinear MPC is used in the high-fidelity verification, the nonlinear optimization problem needs to be solved. Though it is possible to write some nonlinear optimization solver, this will increase the coding complexity. Therefore, using the nonlinear optimization packages such as NLopt [20] and Ipopt [21] would be our choice.

6. CONCLUSION AND FUTURE WORK

6.1 Conclusions

In this report, the preliminary investigation of the passive control system was performed. The investigation was performed based on a simplified reactor dynamics model that was developed in previous work. In the first part of the investigation, the effect of the flow rate was studied. It was shown that the change of flow rate can not introduce reactivity instantaneously. Therefore, the variable flow rate controller is best understood as a delayed control system. The range of the prediction horizon and the weight matrix are very important for successfully characterizing the passive control system with MPC. Parametric studies showed that the MPC can be better applied to the load follow control with power ramp rates smaller than 5% P_0/min.

The second part of the work documented here was the development of the simplified TH model for use in high-fidelity simulations. The model was developed based on the simplified model introduced for the VHTR design [1]. Numerical results showed that the axial temperature distribution calculated by the simplified model agreed well with the SAM results shown in [3], We also layed out a possible scheme to couple the high-fidelity neutronics simulation with the simplified TH model.

The last part of this report described the implementation plan for MPC in the high-fidelity simulation. The plan included possibly obtaining the model forMPC in-line with the high-fidelity transient calculation and before these simulations. Since the simplified dynamics model is nonlinear, it would be helpful to implement the nonlinear MPC controller. Therefore, nonlinear MPC will also be investigated and implemented in the high-fidelity simulation. The solvers that turn the continuous problem to discretized state-space model and the solvers for convex optimization and nonlinear optimization would also be included in our implementation plan.

6.2 Future Work

The major future work includes implementing the feedback model in the high-fidelity simulation and performing both steady-state and transient calculation on some representative problems of the Holos design.

The investigation of the nonlinear MPC in the passive control system based on the simplified model is another important topic for the future work. The work is important to see whether it is possible to have good performance with the passive control system.

Eventually, the MPC controller will be implemented in the high-fidelity simulation, and the performance of the passive control and autonomous control will be more thoroughly investigated.

REFERENCES

[1] C. H. Lee, Z. Zhong, T. Taiwo, W. Yang, H. Khalil, and M. Smith. "Enhancement of REBUS-3/DIF3D for Whole-Core Neutronic Analysis of Prismatic Very High Temperature Reactor (VHTR)." Technical Report ANL-GENIV-076, 917228 (2006).

[2] B. Kochunas, A. Fitzgerald, and E. Larsen. "Fourier Analysis of Iteration Schemes for K-Eigenvalue Transport Problems with Flux-Dependent Cross Sections." *Journal of Computational Physics*, **volume 345**, pp. 294–307 (2017).

[3] V. Seker and B. Kochunas. "Assessment of Local Temperature Reactivity Response in Multi-Module HTGR Special Purpose Reactor." Technical Report NURAM-2020-002-00, University of Michigan, Ann Arbor (2020).

[4] B. Kochunas, K. Barr, and S. Kinast. "Assessment of Variable Reflector Reactivity Envelope in Multi-Module HTGR Special Purpose Reactor." Technical Report NURAM-2020-003-00, University of Michigan, Ann Arbor (2020).

[5] B. Kochunas, K. Barr, S. Kinast, and S. Choi. "Global and Local Reactivity Assessments for Passive Control Systems of Multi-Module HTGR Special Purpose Reactors." Technical Report NURAM-2020-005-00, University of Michigan, Ann Arbor (2020).

[6] S. Choi, S. Kinast, and B. Kochunas. "Point Kinetics Model Development with Predictive Control for Multi-Module HTGR Special Purpose Reactors." Technical Report NURAM-2020-006-00, University of Michigan, Ann Arbor (2020).

[7] R. Hu. "SAM Theory Manual." Technical Report ANL/NE–17/4, 1353375 (2017).

[8] A. Marin-Lafleche, M. A. Smith, and C. Lee. "Proteus-MOC: A 3D Deterministic Solver Incorporating 2D Method of Characteristics." In *Proceedings of ANS MC2013*. Sun Valley, ID (2013).

[9] "ARPA-E | Transportable Modular Reactor." https://arpa-e.energy.gov/technologies/projects/transportable-modular-reactor.

[10] C. Lee, C. Filippone, L. Zou, and N. Stauff. "Core Design of the Holos-Quad Micro Reactor." In *Transactions of the American Nuclear Society - Volume 123*, pp. 1067–1069. AMNS (2020).

[11] C. Filippone, J. Sienicki, L. Zou, and A. Moisseytsev. "Helium Brayton Cycle Design and Analysis for the Holos-Quad Micro Reactor." In *Transactions of the American Nuclear Society - Volume 123*, pp. 1063–1066. AMNS (2020).

[12] C. E. García, D. M. Prett, and M. Morari. "Model Predictive Control: Theory and Practice—A Survey." *Automatica*, **volume 25**(3), pp. 335–348 (1989).

[13] S. P. Boyd and L. Vandenberghe. *Convex Optimization*. Cambridge University Press, Cambridge, UK ; New York (2004).

[14] E. F. Camacho and C. Bordons. *Model Predictive Control*. Advanced Textbooks in Control and Signal Processing. Springer London, London (2007).

[15] N. E. Todreas and M. S. Kazimi. *Nuclear Systems Volume I: Thermal Hydraulic Fundamentals*. CRC Press, Third edition. | Boca Raton : CRC Press, 2021- |, third edition (2021).

[16] H. Petersen. "The Properties of Helium: Density, Specific Heats, Viscosity, and Thermal Conductivity at Pressures from 1 to 100 Bar and from Room Temperature to about 1800 K." Technical Report RISO-224, Danish Atomic Energy Commission (1978).

[17] G. Yang, M. Jaradat, H. Park, W. Yang, and C. Lee. "Multi-Physics Coupling of PROTEUS-NODAL and SAM for MSR Simulation under MOOSE Framework." In *Transactions of the American Nuclear Society - Volume 122*, pp. 647–650. AMNS (2020).

[18] A. Hsieh, G. Zhang, and W. S. Yang. "Consistent Transport Transient Solvers of the High-Fidelity Transport Code PROTEUS-MOC." *Nuclear Science and Engineering*, **volume 194**(7), pp. 508–540 (2020).

[19] L. Grüne and J. Pannek. *Nonlinear Model Predictive Control*. Communications and Control Engineering. Springer London, London (2011).

[20] S. G. Johnson. "The NLopt Nonlinear-Optimization Package." http://github.com/stevengj/nlopt.

[21] A. Wächter and L. T. Biegler. "On the Implementation of an Interior-Point Filter Line-Search Algorithm for Large-Scale Nonlinear Programming." *Mathematical Programming*, **volume 106**(1), pp. 25–57 (2006).